Materials and Design 121 (2017) 109–118

Contents lists available at ScienceDirect

Materials and Design

journal homepage: www.elsevier.com/locate/matdes

The use of femtosecond laser ablation as a novel tool for rapid micro-mechanical sample preparation

Manuel J. Pfeifenberger[a,*], Melanie Mangang[b], Stefan Wurster[c], Jens Reiser[b], Anton Hohenwarter[c], Wilhelm Pfleging[d], Daniel Kiener[c], Reinhard Pippan[a]

[a] Erich Schmid Institute of Materials Science, Austrian Academy of Sciences, Leoben 8700, Austria
[b] Institute for Applied Materials - Applied Materials Physics, Karlsruhe Institute of Technology, Karlsruhe 76021, Germany
[c] Department Materials Physics, University of Leoben, Leoben 8700, Austria
[d] Karlsruhe Nano Micro Facility, Karlsruhe Institute of Technology, Egg.-Leopoldshafen 76344, Germany

HIGHLIGHTS

- A prototype device combining a focused ion beam and a femtosecond laser is presented.
- A case study of fabricating cantilevers for micro-mechanical tests into cold rolled tungsten foils was performed.
- No coarsening of the ultra-fine grained microstructure was found after femtosecond laser ablation.
- A sample array consisting of 100 cantilevers with a dimension of 420×60×25 μm^3 was processed in only half an hour.

GRAPHICAL ABSTRACT

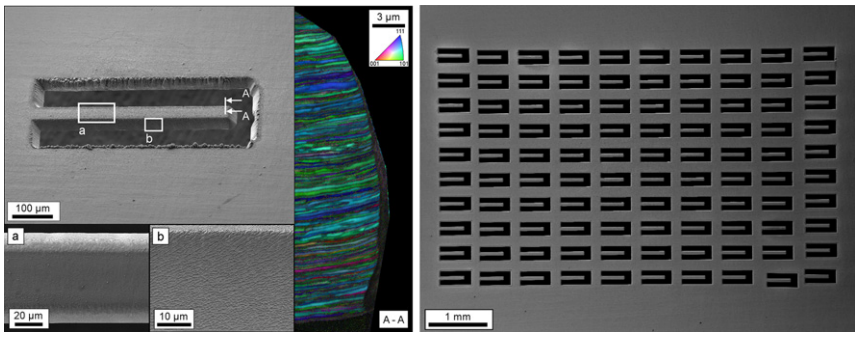

ARTICLE INFO

Article history:
Received 7 December 2016
Received in revised form 2 February 2017
Accepted 6 February 2017
Available online 9 February 2017

Keywords:
Micro-mechanical testing
Femtosecond laser ablation
Nanosecond laser ablation
Sample preparation
Ultra-fine grained tungsten

ABSTRACT

The focused ion beam technique has become a standard tool for micro-mechanical sample preparation in the last decade due to its high precision and general applicability in material removal. Besides disadvantages such as possible ion damage and high operation costs especially the characteristically small removal rates represent a bottleneck for this application. In contrast, femtosecond lasers provide material removal rates orders of magnitude higher, with small or ideally without thermal impact on the surrounding material. Hence, a combination of these two methods offers an ideal tool for time-efficient, micrometer-sized sample preparation. A prototype implementing this idea is presented here in combination with a case study. Cantilevers with a length of several hundred micrometers were machined into 25 μm, 50 μm and 100 μm thick, cold rolled tungsten foils. Scanning electron microscopy analyses reveal the influence of laser parameters and different scanning routines on the resulting sample quality and the effect of the laser pulse length (femtoseconds versus nanoseconds) on the ultra-fine grained microstructure. Finally, the performance for unprecedented rapid sample preparation is demonstrated with a sample array consisting of 100 cantilevers with a dimension of 420×60×25 μm^3 processed in only half an hour, opening completely new testing possibilities.

* Corresponding author.
E-mail address: manuel.pfeifenberger@oeaw.ac.at (M.J. Pfeifenberger).

http://dx.doi.org/10.1016/j.matdes.2017.02.012
0264-1275/

1. Introduction

Mechanical experiments with specimens in the size regime between several hundred nanometers and some hundred micrometers become more and more important in order to achieve a better understanding of local mechanical properties and hence the mechanisms determining the materials' behaviour on these length scales [1–3]. Furthermore, the development and usage of small medical devices, micro-electro mechanical systems and nano-composites increase the relevance of the knowledge of the materials' properties at these small dimensions [4,5]. In addition, novel fundamental research approaches conduct micro-experiments, in order to e.g. validate multi-scale modelling approaches [6] or to determine the controlling mechanism of the brittle-to-ductile transition [7].

The state-of-the-art fabrication technique for the preparation of miniaturized mechanical samples is focused ion beam (FIB) machining. Up to a sample size of few tens of micrometers the FIB technique offers an ideal tool in terms of variability and further provides high precision down to the sub-micrometer domain [8–10]. Utilizing this technique for micro-mechanics provided the basis for the development of various miniaturized testing concepts and sample geometries [11]. For example, for the fabrication of specimens in the micrometer range, starting from thin sheets [12] or bulk materials [13], it presents nowadays a standard tool. Nevertheless, due to the low removal rates it impedes the fabrication of an adequate number of samples when sufficient statistical information is required and therefore becomes a costly and time-consuming method. Hence, the sample preparation employing the FIB technique represents a bottleneck for micro-mechanical studies. A further disadvantage of the FIB is the so-called ion-damage, which describes ion-induced defects in the near-surface layer caused by ion implantation [14,15].

Especially the pre-preparation of samples usually requires the removal of a large amount of material and therefore is a time critical step. Due to the depletion of the ion source, these time intensive rough cuts make up a significant part of the operation expenses for a FIB system. High currents further lead to a high ion beam dosage and hence a strong influence on the material [16].

Wurster et al. [17] showed how the FIB cutting time can be considerably reduced by employing the ion slicing technique for the pre-preparation of test specimens. Additionally, this reduces the ion-induced damage in comparison to pure FIB milling. This damage reduction is based on a lower acceleration voltage and the use of argon instead of gallium ions. However, there are still various disadvantages of the ion slicing technique. An irradiation damage may occur, the thickness of the specimen is limited to few microns only, an adequate masking technique has to be applied and complex geometries are difficult to fabricate [17].

Another technological advancement regarding the reduction of the FIB processing time is the application of recently developed xenon plasma sources for micro-machining [18]. It enables faster material removal due to 1–2 orders of magnitude higher milling currents compared to the gallium FIB [19]. More recent studies also suggest that the influence on the mechanical properties of the processed material is less pronounced. Kwakman et al. noticed that the extent of the damage layer is reduced by approx. 25% [20]. Micro-compression experiments on polycrystalline aluminium performed by Xiao et al. [21] using pillars fabricated by a xenon and a gallium FIB exhibited a lowered yield strength for the samples prepared by the gallium FIB. However, the size of structures machinable with the xenon FIB is still limited to a few hundred micrometers.

On the meso-scale, i.e. in the range of 100 to 10,000μm a precise and versatile method for sample preparation with limited influence on the material is not available. Suitable methods for these dimensions, such as micro-electrical discharge machining (μ-EDM) or micro-machining, influence the material either through heat or through plastic deformation. Kawakami et al. observed the generation of residual stresses in tungsten micro-beams due to the thermal impact of the μ-EDM cutting process [22]. The fabrication of micro-mechanical samples with μ-EDM has been conducted for example by Schmitt et al., producing micro-cantilevers [23], or Uchic et al., producing micro-compression samples [24]. For these specimens an additional preparation step was required due to the rough surface and the heat affected zone resulting from the μ-EDM processing. In [23] a FIB was employed to notch the cantilevers and to polish the cutting edges nearby the notch. Additional disadvantages of μ-EDM are the required fabrication of the electrode (for sinking μ-EDM), the subsequent wear of the electrode during processing, as well as the limitation of the technique to conductive materials [25].

Another widely used method for machining specimens on this small scale are lasers. Investigations on the capability of the laser for micro-machining started shortly after its invention [26]. However, the heat influence of continuous wave or short pulse (pulse duration $>$ 10 ps [27]) lasers impedes the processing of sharp, well defined geometries [28] and therefore their applicability for micro-machining has been limited to cases, where a possible modification of the material is not critical. In contrast, ultrashort pulsed lasers (pulse duration $<$ 10 ps) enable laser micro-machining of well defined geometries with a very good reproducibility [28,29]. In recent investigations it has been shown that ultrashort pulsed laser materials processing achieved a high reliable standard which enables this technology to enter new and advanced industrial applications [30–32]. This is due to the fact that the laser pulse duration is significantly below the heat diffusion time ($>$10–100 ps). The ultrashort pulse duration and the high intensity on the material surface lead to complete ionization of the irradiated material by non-linear effects. The irradiated material volume is removed from the surface before any heat diffusion or thermal damage and melting can occur.

When the laser beam is guided in parallel incidence to the ablated surface, the Gaussian intensity distribution of the laser beam [29] ensures that the ablation of the material happens at the threshold fluence, leading to optimal surface quality. On the other hand when the beam is guided perpendicularly to the ablated sample surface the resulting surface quality is lower and strongly depends on the applied process parameters. Further, a perpendicular incidence leads to an increased creation of dislocations and their density scales with the peak fluence of the laser pulse. For a parallel incidence the depth of the dislocation zone is significantly reduced [27]. In this case a high dislocation density is found within few 100 nm of the processed surface [33]. A similar dependence on the incidence angle has been found for the ion damage of FIB processing [14]. Femtosecond laser processed silicon exhibited an amorphized layer near the surface, extending 50 nm in depth [33].

With the advent of reliable ultrashort pulsed lasers their unique properties found wide interest in science and industry, and several applications have been developed since then. The various possibilities to structure and modify surfaces [34] can be used e.g. to tune optical properties of metal surfaces [35] or to reduce the reflectivity

Table 1
Specifications of the three laser sources which were used in this study.

	Laser I	Laser II	Laser III
t_p	0.35–10 ps	4–20 ns	318 fs
P_{max} [W]	20	2.2	4
R_{max} [MHz]	2	0.12	1
λ [nm]	1030, 515, 343	355	1030, 515, 343
d_0 [μm]	35	27	25

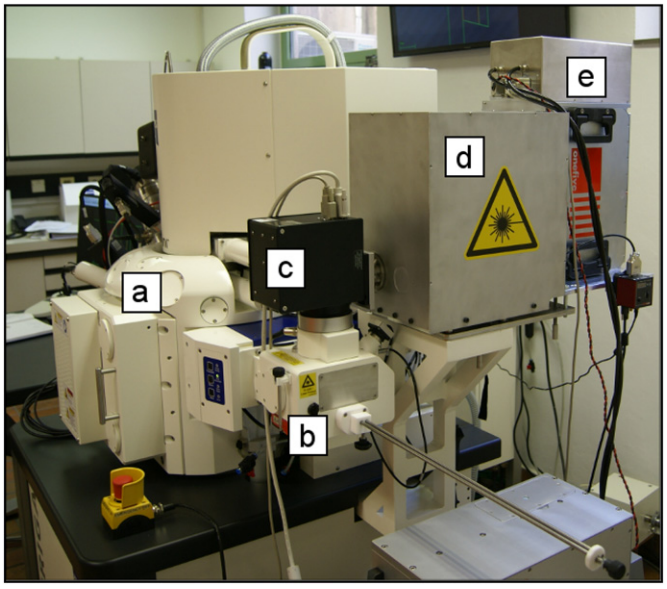

Fig. 1. System setup with main FIB/SEM chamber (a), laser processing chamber (b), scan unit (c), optical unit (d) and femtosecond laser unit (e).

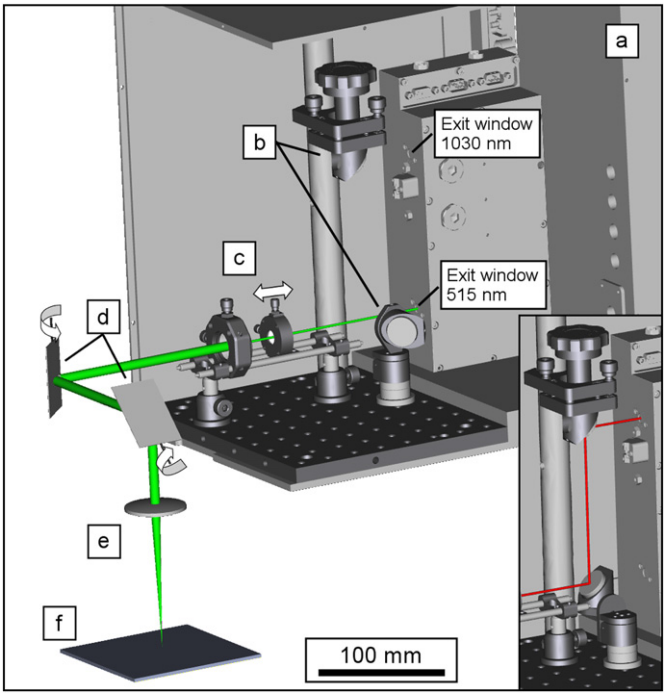

Fig. 2. Detailed view of the beam path starting from the laser unit (a) along the beam expander (c), the mirrors of the scanning unit (d) and the objective lens (e). The exit windows for the wavelengths of 515 nm and 1030 nm are located on different heights. The periscope (b) optionally guides the beam with a wavelength of 1030 nm into the beam expander (shown in inset).

of silicon photovoltaic cells [36]. Furthermore, due to the feasibility of ablating various materials, the capability for micro-machining of ultrashort pulsed laser ablation has been investigated for e.g. metals [37–39], biomaterials [40,41], dielectrics [42], semiconductors [43,44] or polymers [45].

Comparing the laser ablation to the standard gallium FIB technique, its ablation rate is 4–6 orders of magnitude higher. Also the ablation rate of a xenon FIB is still 2–3 orders of magnitude below the achievable rates of an ultrashort pulsed laser [27]. However, compared to the FIB the laser exhibits a reduced precision. One reason for this is the large spot diameter of approximately 25 μm, which is due to the scan optics setup used in this study. It is approx. 3 orders of magnitude larger than the spot size of a gallium FIB at 1 nA [19]. By using fixed optics and a positioning stage the precision can be improved. A main challenge that arises when samples are prepared with the ultrashort pulsed laser is the creation of so-called laser induced periodic surface structures (LIPSS). These LIPSS are an inherent feature of ultrashort pulsed laser processing. An overview of the size and orientation of the ripple-like structures for different materials is given in [46]. For linear polarized light the ripples are mostly oriented perpendicularly to the polarization of the laser [46]. For circular polarization the surface features exhibit a dot-like structure [47].

Due to the high precision of the FIB technique and the high ablation rates of the ultrashort pulsed laser technique, a combination of both methods yields a powerful device for machining from the micro- to the meso-scale. The addition of a scanning electron microscope (SEM) allows for an immediate analysis of the processed specimens. Such a combination has already been realised by Echlin et al. [27,48]. They built a setup for femtosecond laser ablation in-situ in a SEM to perform rapid 3D material analysis. A further assessment of combining the nano- or femtosecond laser technique with either a xenon or a gallium FIB has been conducted by Kwakman et al. [20].

As outlined before, the properties of ultrashort pulsed lasers are appealing for the fabrication of micro-mechanical test samples. To date, this application has been rarely investigated. Lim et al. studied the fabrication of micro-pillars on bovine cortical bone [41]. Very recently, in macroscopic mechanical tests femtosecond lasers have been successfully employed for introducing notches into single edge notched beam samples [49,50].

The aim of this paper is to establish and to assess femtosecond (ultrashort) pulsed laser processing as a novel technique for the fabrication of micro-mechanical samples. In the following an overview of the combined SEM/FIB - femtosecond laser system is given. Then

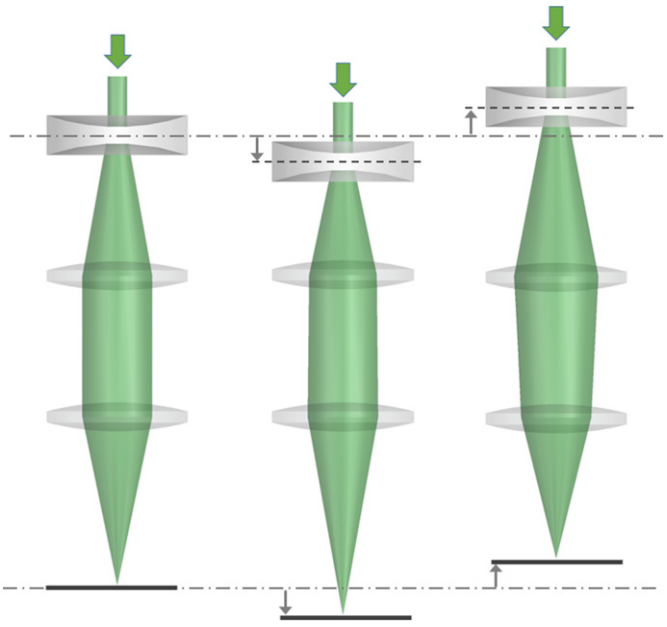

Fig. 3. Working principle of the beam expander. Changing the distance between the dispersal and the subsequent collecting lens, varies the position of the focal plane.

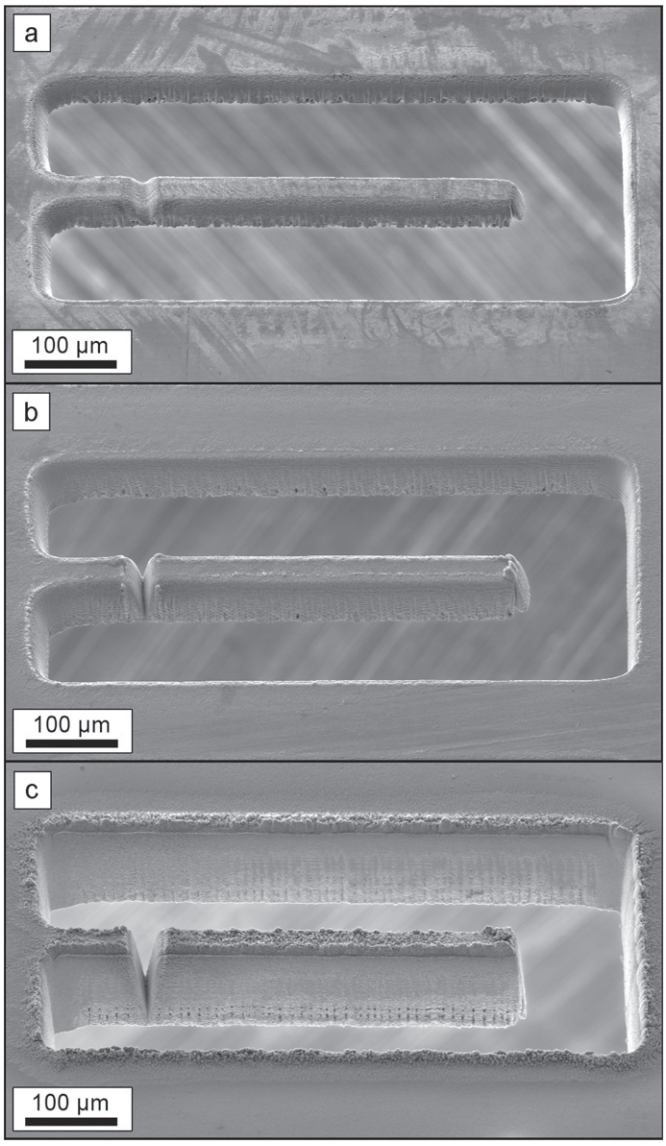

Fig. 4. Cantilevers cut with a femtosecond laser (KIT-KNMF) in foils with (a) 25 μm, (b) 50 μm and (c) 100 μm thickness. The used scan pattern is shown in Fig. 5a. The number of scan passes are listed in Table 2. For these samples also the notch was laser processed.

the performance of the femtosecond laser for the fabrication of micro-cantilevers is assessed and process parameters are optimized in terms of redeposition and surface quality. In addition, the quality and the microstructure of samples processed by nanosecond and femtosecond laser radiation is compared. Finally, the question if femtosecond laser micro-machining allows the mass-production of micro-mechanical samples is answered.

2. Experimental

In this study three different pulsed laser sources were used. The specifications of these lasers are summarized in Table 1. The specifications include the maximum average power P_{max}, the wavelength λ, the maximum pulse repetition rate R_{max} and the pulse duration t_p.

Initial investigations have been performed at the Karlsruhe Institute of Technology at the Karlsruhe Nano Micro Facility (KNMF) by employing a micro-machining workstation (PS450-TO, Optec, Frameries, Belgium). This workstation is equipped with an ultrashort pulsed laser (Tangerine, Amplitude Systèmes, Pessac, France - Laser I in Table 1). The laser beam is scanned across the sample surface employing a scan head (RhotorTM Laser Deflection Systems, Newson Engineering BV, Dendermonde, Belgium) and finally focused by a f-theta lens with 100 mm focal length.

Table 2
Parameters for the cantilevers cut in foils with different thicknesses using a femtosecond laser with a wavelength of 1030 nm and a laser pulse duration of 380 fs (Laser I in Table 1). The resulting samples are shown in Fig. 4.

Foil thickness	25 μm	50 μm	100 μm
Fluence [J/cm^2]	0.7	1.0	1.6
Repetition rate [kHz]	20	20	40
Scan speed [mm/s]	100	100	50
Scan repetitions	150	300	400

Further tests and analyses have been conducted using a femtosecond laser system at the Erich Schmid Institute of Materials Science and the Materials Physics Department of the University of Leoben.

2.1. System design

The basis of the new femtosecond laser system is the Auriga Laser platform (Zeiss, Oberkochen, Germany - concept of the platform see [51]). The modified setup is displayed in Fig. 1. It consists of two vacuum chambers separated via an airlock. The main chamber (Fig. 1 - a) contains the FIB and the SEM gun in a standard cross beam implementation. The laser processing is conducted in the separated second chamber (Fig. 1 - b). Both chambers as well as the laser unit (Fig. 1 - e) and all optical components are mounted on the same active air suspension for damping. The separation of the two chambers has the advantage that the high amount of ablated material during the laser processing does not contaminate the main chamber. Nevertheless, this setup allows femtosecond laser processing and successive SEM analysis or FIB cutting without leaving the vacuum state. An additional advantage is the possibility to use the laser in air or under inert gas conditions. This is especially of great interest, when working on bio-materials.

The nanosecond laser (Laser II in Table 1) originally used in the commercial Zeiss system is replaced by a femtosecond laser (Origami 10 XP, Onefive GmbH, Regensdorf, Switzerland - Laser III in Table 1).

A look into the optical unit (Fig. 1 - d) and the scan unit (Fig. 1 - c) provides details on the beam path (Fig. 2). The orientation of the laser unit causes that the separate exit windows of the three wavelengths are located on different height levels. By employing a periscope (Fig. 2 - b) equipped with mirrors, designed for femtosecond laser pulses, all beams are guided along the same path through the beam expander (Fig. 2 - c). The lower mirror of the periscope can be moved into and out of the beam path by a flip mount. The mirror positioned in the beam path is shown in the inset in Fig. 2. After passing the beam expander, the laser beam is guided into the processing chamber via a scan unit (intelliscan III 10, SCANLAB AG, Puchheim, Germany), employing two perpendicularly oriented femtosecond mirrors (Fig. 2 - d), which are driven by galvanometers. This scan unit allows for a scanning area of 50 × 50 mm^2 and a relative positioning accuracy of about 0.3μm at the sample surface. The scanning principle enables the fabrication of arbitrary geometries, which are defined using a computer-aided design programme. The objective lens which finally focuses the laser beam onto the sample is a f-theta lens (Sill Optics GmbH, Wendelstein, Germany) ensuring a flat image plane and therefore a constant focal width across the scan area (Fig. 2 - e, f). The used objective has a working distance of 145.7 mm. The focal diameter on the sample is adjusted by the beam expander, consisting of an uncoated dispersing lens and an uncoated collecting lens, located between the periscope and the scan unit. The position of the minimal focal diameter is defined by the distance between these two lenses (Fig. 3). The position of the dispersal lens can be varied and is controlled by a stepper motor actuator. This setup allows a

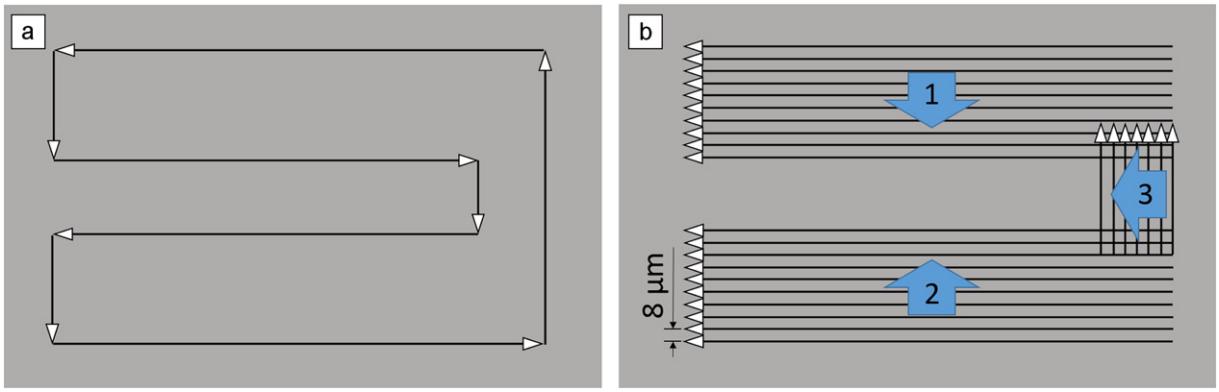

Fig. 5. The scan routines for the fabrication of cantilevers. The U-shape can either be cut out by a single contour cut (a) or by removing the whole material by scanning across the respective area (b). The narrow arrows indicate the lines of the laser cuts and the broad arrows indicate the scan direction.

shift of the position of the minimal focal diameter of approximately 30 mm and therefore allows the same variance in sample height.

The laser system offers five parameters to be adjusted: The average laser pulse power and the laser pulse repetition rate. Further, a shutter allows to adjust the number of transmitted pulses. In addition, the laser scanning speed across the sample surface and the number of repetitions of each laser scan line are variable.

A spot size evaluation on the modified system was performed according to [52]. The determined spot diameter was $24.5 \pm 0.3\mu$m. The ablation threshold fluence yielded 0.20 ± 0.01 J/cm^2 for the tungsten foils. This is in good agreement with Byskov-Nielsen et al. [53], considering the linear dependence of the threshold fluence on the wavelength for sub-picosecond pulses [54]. Byskov-Nielsen et al. [53] found for tungsten a single pulse threshold of 0.44 ± 0.02 J/cm^2 for femtosecond laser ablation with a wavelength of 800 nm. The same analysis for the nanosecond laser operating with a wavelength of 355 nm provided a spot diameter of 27.4 ± 1.9 μm and a fluence threshold of 5.8 ± 1.0 J/cm^2. This threshold value agrees well with the values listed in [55], where thresholds of 8.32 J/cm^2 and 4.28 J/cm^2 were found for wavelengths of 266 nm and 532 nm respectively.

2.2. Material and methods

In this study cold rolled tungsten foils with a thickness of either 25μm, 50μm or 100μm were used as sample material. These foils exhibit an ultra-fine grained microstructure and excellent ductility. Therefore, they are promising for the use as structural material in high temperature applications [56]. The enhanced mechanical properties are governed by the microstructure of the foil. It is of great importance to prevent the material from being damaged by melting, recrystallization or by crack formation during preparation [56]. Therefore, the use of a femtosecond laser seems to be an appropriate tool in order to avoid a thermal impact on the material during the ablation process. Tungsten additionally represents a challenging material for FIB processing due to its low sputter yield [57] and is therefore an ideal example for the investigation of the ablation capability and efficiency of a femtosecond laser. Cantilevers are a widely used specimen type for micro-mechanical testing, hence, this geometry has been selected to study the performance of the new system.

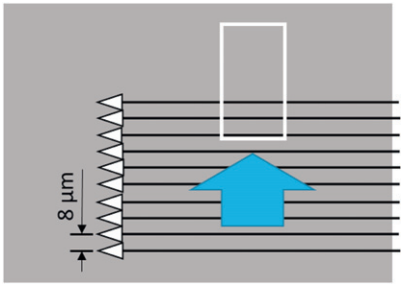

Fig. 6. The scan pattern for the parameter tests. The horizontal arrows indicate the lines of the laser cuts and the broad arrow the scan direction. The white rectangle marks the area of interest shown in Fig. 7. The pattern was located on the edge of the foil.

For the electron backscatter diffraction (EBSD) data acquisition a scanning electron microscope (LEO 1525, Zeiss, Oberkochen, Germany) with an EBSD detector (EDAX Inc., New Jersey, USA) was used. The data was analysed with the EDAX OIM Data Analysis software. For the scans a step size of 50 nm and an acceleration voltage of 20 kV was chosen.

3. Results and discussion

3.1. Scanning routine and parameter optimization

The initial tests at KIT-KNMF demonstrated the feasibility of femtosecond laser processing for the production of micro cantilevers made of tungsten. Samples were cut into foils, fabricated by cold rolling, with thicknesses of 25μm, 50μm or 100μm. Fig. 4 shows cantilevers cut through the thickness of these foils. The laser parameters used for these samples are listed in Table 2. The respective scan pattern is displayed in Fig. 5a. The same pattern was scanned multiple times to ensure full penetration. The number of scan repetitions is given in Table 2. In these samples also a notch was introduced using the femtosecond laser. Because of the significantly larger tip radius compared to a FIB notch, the laser processing of notches has not been further investigated in this study.

In the used configuration the laser beam is oriented perpendicularly to the foil. Therefore, the incidence of the laser beam with respect to the ablated material is normal at the beginning of the process. After the penetration of the foil a glancing incidence is achieved.

The cutting edges exhibited a wavy structure towards the bottom. Particularly for the 100 μm thick sample an array of cavities is observed. This is on the one hand due to a non-optimal overlap of successive laser pulses, because of the high scanning speeds used for the 25 μm and 50 μm samples. On the other hand, cutting only the contour of the desired shape, as shown in Fig. 5a, is unfavourable for an increasing foil thickness because the redeposited material from preceding scanning steps increasingly hinders material transport away from the processing region and therefore impedes an even

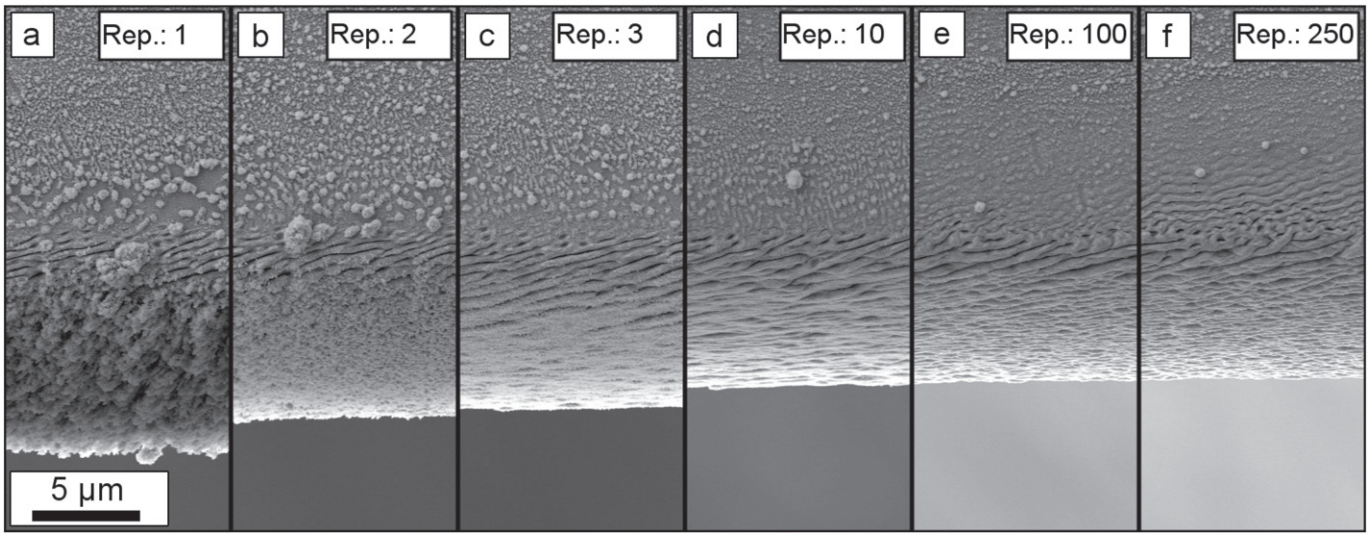

Fig. 7. Samples cut in a 25 μm thick foil using the scan pattern in Fig. 6 with a different number of repetitions per scan line in a single pass. Increasing the number of repetitions leads to a smoother cut edge and a reduced taper angle (a)–(c), but also to the occurrence of LIPSS on the top face of the sample for higher repetition numbers (e), (f).

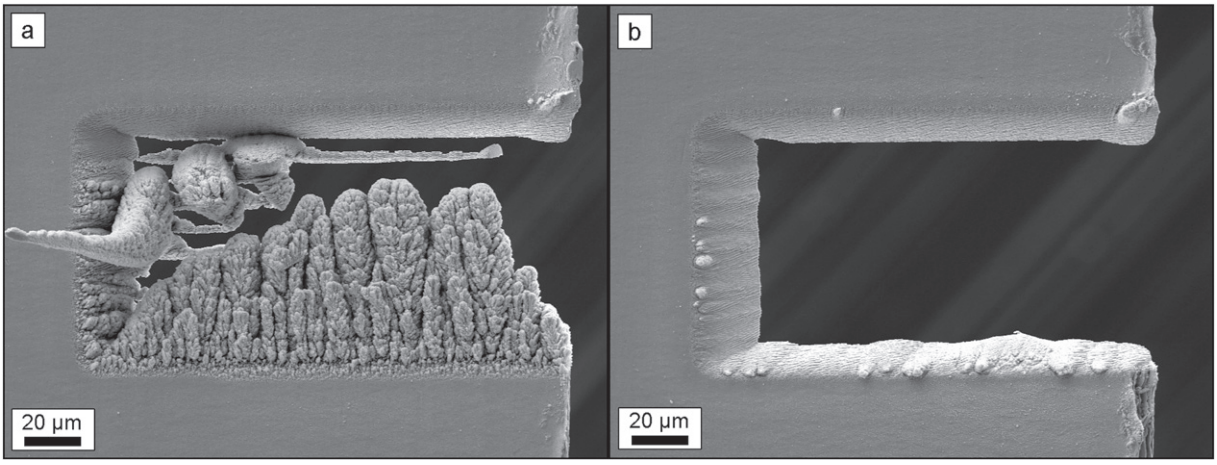

Fig. 8. The scan pattern displayed in Fig. 6 is cut into a foil with a thickness of 25 μm. (a) Single pass scanning with 20 repetitions per line leads to an extensive redeposit of ablated material. (b) Multiple pass scanning (5 repetitions per line and 4 passes) minimizes redeposition.

ablation. Further, the U-shaped remnant piece will move or fall out during the last scan repetitions and thus change the conditions for the interaction of the laser with the material. The remnant piece can remain stuck, especially in thicker foils, and has to be removed via a follow-up treatment. Though, the scan pattern in Fig. 5a yields the lowest scan time for the intended cantilever geometry. The generation of debris on the surface lowers the surface quality as displayed in Fig. 4. Shaheen et al. found for an increasing fluence an increase in the amount of generated debris. Further re-solidified molten material occurs at high fluences, though, none was observed in the low fluence regime [58]. For an increasing foil thickness, more ablated material and therefore more debris on the top face of the cantilever was found. The generated debris leads to a change of colour around the processed area. However, it can be removed nearly completely by cleaning the sample in a ultrasonic bath filled with soap water.

To further enhance the surface quality of the cutting edge a second scan pattern has been applied. It is displayed in Fig. 5b. Using this scan pattern also avoids any remnant piece of getting stuck, because here the whole U-shape is removed during processing. Nevertheless, due to the ablation of a larger amount of material more debris is generated.

With the modified prototype multiple scanning routines and parameter tests were performed to identify their influence on the resulting sample. The 25 μm thick foils served as samples for these experiments. Fig. 6 shows the rectangular scan pattern employed for these experiments. The pattern has been chosen with the goal to remove a certain area of the sample to successively enable the fabrication of free-standing specimens. Starting from the lower right corner each line is scanned from right to left. After a certain number of repetitions per line the beam moves to the next upper line. In total 10 lines with a distance of 8μm in between were cut. A distance of 8μm ensures sufficient overlap between the lines. This pattern was

Table 3
Parameters of the lasers used for the fabrication of the cantilevers displayed in Fig. 9 and Fig. 10.

	Laser II (ns-laser)	Laser III (fs-laser)
Fluence [J/cm^2]	15.3	1.1
Repetition rate [kHz]	25	100
Scan speed [mm/s]	60	10

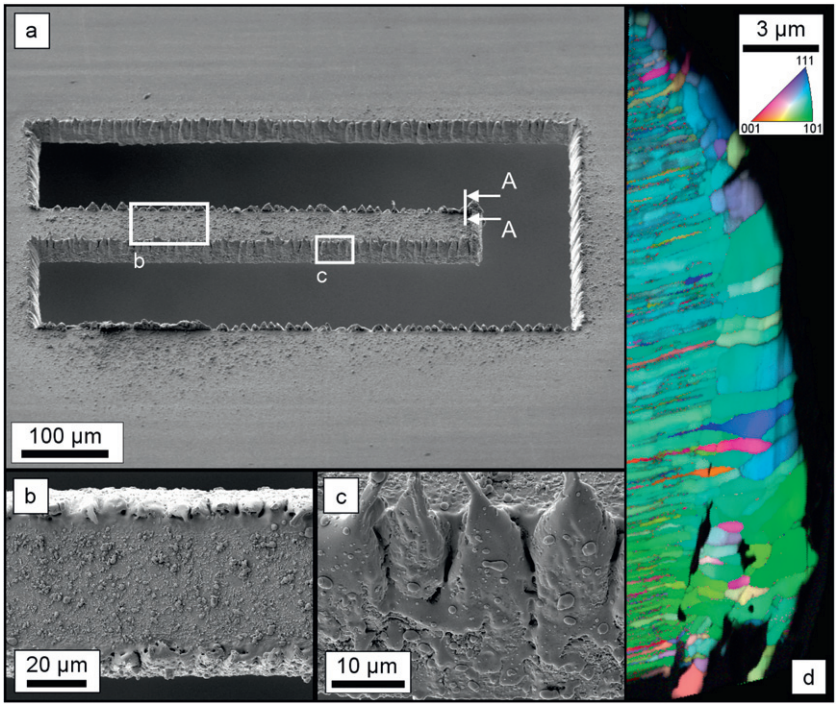

Fig. 9. A cantilever fabricated by a nanosecond laser in a foil with a thickness of 25 μm is displayed in (a). The scan pattern in Fig. 5a was scanned in 2 passes. The magnified top view (b) shows rough debris. The magnification of the cut edge shows a melted surface and a distinct burr (c). An EBSD analysis of the cross-section A-A indicated in (a) reveals coarsened and equiaxed grains in the heat influenced zone (d). The inset triangle shows the colour coding of the crystal orientation with respect to an external reference.

used to create the cuts shown in Fig. 7 and Fig. 8. For these tests a laser fluence of 1.1 J/cm^2, a scan speed of 1 mm/s and a laser pulse repetition rate of 100 kHz have been used.

The micrographs in Fig. 7 display the cut edges on the top side of the scan pattern as indicated by the white rectangle in Fig. 6. These cuts were fabricated with a repetition number of 1, 2, 3, 10, 100, 250 for each line. It was found that for this parameter set with 10 line repetitions the surface quality of the cut edge does not significantly increase any more. For higher repetition numbers periodic structures also start to form on the top face of the sample (Fig. 7 (e), (f)).

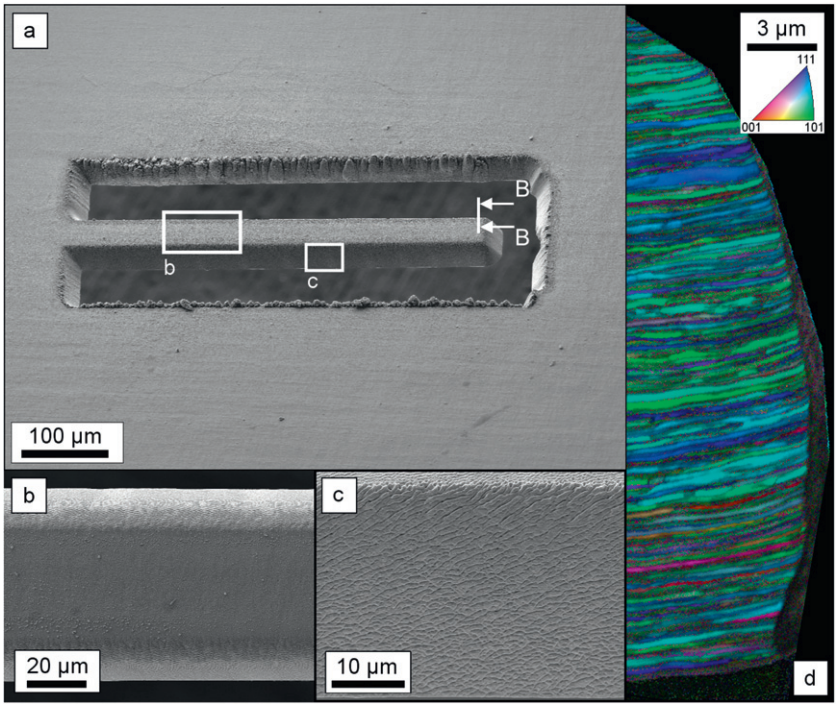

Fig. 10. A cantilever fabricated by a femtosecond laser in a foil with a thickness of 25 μm is shown in (a). The scan pattern in Fig. 5b was scanned in 2 passes with 5 repetitions per line. In the magnified top view (b) less debris is found than for the nanosecond laser processing. The magnification of the cut edge exhibits the characteristic laser induced periodic structures (c). An EBSD analysis of the cross-section B-B indicated in (a) reveals no grain coarsening near the cut edge (d). The inset triangle shows the colour coding of the crystal orientation with respect to an external reference.

Besides enhancing the surface quality of the cut edges, also the amount of redeposited material needs to be reduced. In Fig. 8 the processed areas are viewed in total. For the cut in Fig. 8a each line of the scan pattern was repeated 20 times. It exhibits a significant redeposition of ablated material on the lower edge. For the sample in Fig. 8b each line of the scan pattern was repeated 5 times and additionally the whole scan pattern (Fig. 6) was repeated in 4 passes. These tests exhibited that multiple passes significantly reduce the amount of redeposited material. This strategy is well known for the FIB technique, where multiple pass scanning is applied to minimize material redeposition [57].

A variation of the average laser power showed that after the power suffices to penetrate the foil a further increase leads initially to a decrease of the taper angle at the cut edges. Finally, a saturation of the taper angle is observed with increasing laser power.

The findings in this section were considered when designing the scanning routine and choosing the parameters for the cantilever fabrication. For larger samples a combination of the patterns in Fig. 5a and Fig. 5b can be favourable, using first a contour shape for a rough cut followed by few parallel cuts to enhance surface quality of desired edges. This way the processing time required, when using the principle of the pattern in Fig. 5b, can be reduced.

3.2. Comparison of nanosecond and femtosecond laser processing

In this section the results of processing with a nanosecond (Laser II in Table 1) and a femtosecond laser (Laser III) are compared. The surface quality of the cut edges as well as the influence of the laser pulse duration on the microstructure were investigated. The process parameters are displayed in Table 3. Although the average power of the nanosecond laser is higher, the peak power of the femtosecond laser pulses, due to the much smaller pulse duration, is approx. 3 orders of magnitude higher. For the nanosecond laser processing the scan pattern in Fig. 5a was scanned in 2 passes. For the femtosecond laser processing the pattern in Fig. 5b was scanned in 2 passes with 5 repetitions per line.

Fig. 9a shows a cantilever processed with the nanosecond laser. Machining with the nanosecond laser leads to extensive debris formation on the top face (Fig. 9b). This redeposition is produced by the ejection of molten material [58]. The surface of the cut edge shows melted structures and a distinct burr as displayed in Fig. 9c. Fig. 10a shows a cantilever processed with the femtosecond laser. Compared to the nanosecond laser machining less and smaller debris is generated on the top face (Fig. 10b). Further, the cut edge of the femtosecond laser cut is smoother and no burr can be found (Fig. 10a and c). Although the surface quality is improved employing femtosecond laser pulses, a completely structure free surface cannot be obtained due to the occurrence of the characteristic LIPSS (Fig. 10c).

Investigations of the microstructure underneath the edge of the laser cut yield a significant difference between the samples processed with the nanosecond and the femtosecond laser, respectively. Inverse pole figure maps were obtained from EBSD analyses of FIB polished surfaces which were oriented perpendicular to the laser cut. The results are presented in Fig. 9d and Fig. 10d. The inset shows the colour coding of the EBSD pattern, which describes the crystal orientation with respect to an external reference. The greyscale of the maps has been coded with the image quality. Due to the rolling fabrication of the tungsten foils the grains initially feature an elongated structure with a grain thickness of approximately 300–500 nm and a high defect density giving rise to a low grey value. The microstructure of the nanosecond laser processed samples exhibits coarsened, nearly equiaxed grains in the vicinity of the cut edge (Fig. 9d). The coarsening can be explained by a recrystallisation process, which followed after the heat influence exerted by the nanosecond laser pulses. For the employed parameter set coarsening is found up to approximately 4 μm underneath the cut surface. Furthermore, due to the recrystallisation the defect density is reduced, resulting in a brighter image. On the contrary the femtosecond laser processed samples show no change in the grain shape and in the EBSD pattern quality due to recovery as shown in Fig. 10d.

To evaluate the extent of the periodic surface structures a FIB cross-section located on the cut edge was analysed as shown in Fig. 11. The LIPSS show a periodicity of about 250 nm and a depth of about 100 nm. This is in good agreement with the LIPSS dimensions Echlin et al. [33] found for various materials. Furthermore, the microstructure a few tens of nm underneath the LIPSS reveals no change. While representing no impediment for example for tensile testing of ductile materials, this surface roughness will inhibit such tests for brittle materials. Nevertheless, for fracture experiments the LIPSS will be of no relevance, because the required notch depth exceeds their dimension by far.

Fig. 12 emphasizes the efficiency of the femtosecond laser system for sample preparation. The cantilever shown in Fig. 12a was fabricated using the laser, while the notch was introduced employing the FIB. The laser processing step takes approximately 20 s. A set consisting of 100 cantilevers with a dimension of $420\times60\times25$ μm^3, as shown in Fig. 12b, takes therefore only about half an hour. The complete machining by FIB would require about 1 year of continuous milling, assuming a high ablation rate of 10 $\mu m^3/s$.

4. Conclusions

In this study, the feasibility of employing a femtosecond laser for the rapid fabrication of micro-mechanical test structures, in the particular case cantilevers in tungsten foils, with lengths up to several hundred micrometers has been demonstrated. For this purpose a device combining a FIB and a SEM in a standard crossbeam implementation and a nanosecond laser was modified to be operated with a femtosecond laser. The system enables fast material removal by a femtosecond laser and precise FIB end-processing as well as scanning electron analyses without any need of interrupting the vacuum conditions. Furthermore, the system design with a separated laser chamber allows processing in air or under certain inert gas conditions, which is of interest when e.g. working on bio-materials. The femtosecond laser processing enables a material independent ablation without significant heat impact on the surrounding material. Employing a scan unit to move the beam across the sample offers fast processing and a high variability in sample geometries, for example round pillars or tensile specimens.

The authors believe that this novel method will find wide application for unprecedented fast pre-preparation and preparation of

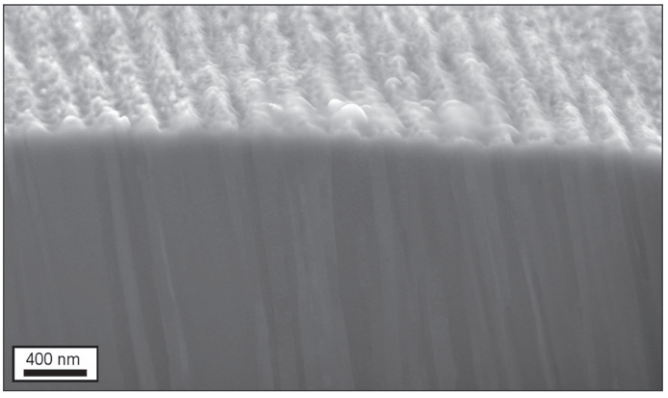

Fig. 11. A FIB cross-section through the LIPSS on the cut edge shows a periodicity of the undulating structures of approximately 250 nm. The depth is about 100 nm. The elongated grains due to the rolling fabrication are visible and reveal no change in structure underneath the LIPSS.

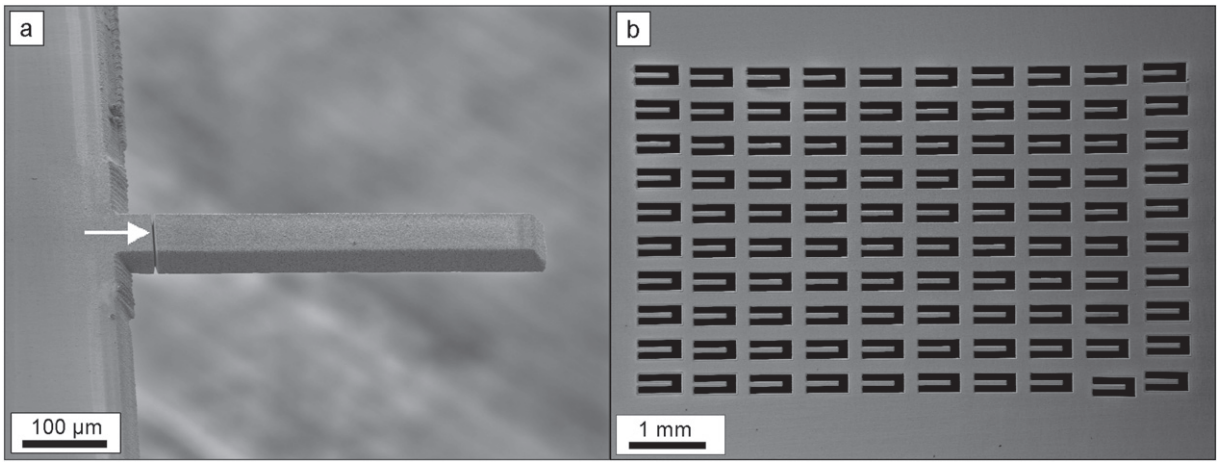

Fig. 12. (a) Femtosecond laser cut cantilever with a notch introduced by a FIB (indicated by white arrow). (b) The micrograph shows 100 cantilevers with a length of 420 μm and a width of 60 μm prepared in only half an hour in a tungsten foil with 25μm thickness.

samples on the micro-scale. Furthermore, it represents a unique and versatile tool for producing samples in the meso-scale up to few 10 mm dimensions. The rapid processing can be regarded as a mass production technique for micro samples and therefore helps to facilitate the acquisition of sufficient statistical information for micro-mechanical experiments. It will contribute to relieve the bottleneck posed by the established FIB technique for micro-mechanical sample preparation and testing.

Acknowledgements

KIT has received funding from the European Union's Horizon 2020 research and innovation programme under the Marie Sklodowska-Curie grant agreement no. 644971. In addition, the support for femtosecond laser processing by the Karlsruhe Nano Micro Facility (http://www.knmf.kit.edu/), a Helmholtz research infrastructure at KIT is gratefully acknowledged.

The authors thank the Zeiss team in Oberkochen, especially Dr. Hiller, for their support in issues regarding the modification of the Zeiss Auriga Laser.

References

[1] J.R. Greer, J.T.M. De Hosson, Plasticity in small-sized metallic systems: intrinsic versus extrinsic size effect, Prog. Mater. Sci. 56 (6) (2011) 654–724. http://dx.doi.org/10.1016/j.pmatsci.2011.01.005.
[2] M.D. Uchic, D.M. Dimiduk, J.N. Florando, W.D. Nix, Sample dimensions influence strength and crystal plasticity, Science 305 (5686) (2004) 986–989. http://dx.doi.org/10.1126/science.1098993.
[3] M.D. Uchic, P.A. Shade, D.M. Dimiduk, Plasticity of micrometer-scale single crystals in compression, Annu. Rev. Mater. Res. 39 (1) (2009) 361–386. http://dx.doi.org/10.1146/annurev-matsci-082908-145422.
[4] A.C.R. Grayson, R.S. Shawgo, A.M. Johnson, N.T. Flynn, Y. Li, M.J. Cima, R. Langer, A BioMEMS review: MEMS technology for physiologically integrated devices, Proc. IEEE 92 (1) (2004) 6–21. http://dx.doi.org/10.1109/JPROC.2003.820534.
[5] S.A. Wilson, R.P.J. Jourdain, Q. Zhang, R.A. Dorey, C.R. Bowen, M. Willander, Q.U. Wahab, M. Willander, S.M. Al-hilli, O. Nur, E. Quandt, C. Johansson, E. Pagounis, M. Kohl, J. Matovic, B. Samel, W. van der Wijngaart, E.W.H. Jager, D. Carlsson, Z. Djinovic, M. Wegener, C. Moldovan, R. Iosub, E. Abad, M. Wendlandt, C. Rusu, K. Persson, New materials for micro-scale sensors and actuators: an engineering review, Mater. Sci. Eng. R. Rep. 56 (16) (2007) 1–129. http://dx.doi.org/10.1016/j.mser.2007.03.001.
[6] N.M. Ghoniem, E.P. Busso, N. Kioussis, H. Huang, Multiscale modelling of nanomechanics and micromechanics: an overview, Philos. Mag. 83 (2003) 3475–3528. http://dx.doi.org/10.1080/14786430310001607388.
[7] H. Li, F. Ebrahimi, Ductile-to-brittle transition in nanocrystalline metals, Adv. Mater. 17 (16) (2005) 1969–1972. http://dx.doi.org/10.1002/adma.200500436.
[8] M.W. Phaneuf, Applications of focused ion beam microscopy to materials science specimens, Micron 30 (3) (1999) 277–288. http://dx.doi.org/10.1016/S0968-4328(99)00012-8.
[9] J. Melngailis, Focused ion beam technology and applications, J. Vac. Sci. Technol. B 5 (2) (1987) 469–495. http://dx.doi.org/10.1116/1.583937.
[10] C.A. Volkert, A.M. Minor, Focused ion beam microscopy and micromachining, MRS Bull. 32 (5) (2007) 389–399. http://dx.doi.org/10.1557/mrs2007.62.
[11] D. Kiener, C. Motz, G. Dehm, R. Pippan, Overview on established and novel FIB based miniaturized mechanical testing using in-situ SEM, Int. J. Mater. Res. 100 (8) (2009) 1074–1087. http://dx.doi.org/10.3139/146.110149.
[12] J. McCarthy, Z. Pei, M. Becker, D. Atteridge, FIB micromachined submicron thickness cantilevers for the study of thin film properties, Thin Solid Films 358 (12) (2000) 146–151. http://dx.doi.org/10.1016/S0040-6090(99)00680-X.
[13] D. Di Maio, S. Roberts, Measuring fracture toughness of coatings using focused-ion-beam-machined microbeams, J. Mater. Res. 20 (02) (2005) 299–302. http://dx.doi.org/10.1557/JMR.2005.0048.
[14] D. Kiener, C. Motz, M. Rester, M. Jenko, G. Dehm, FIB damage of Cu and possible consequences for miniaturized mechanical tests, Mater. Sci. Eng. A 459 (12) (2007) 262–272. http://dx.doi.org/10.1016/j.msea.2007.01.046.
[15] S. Rubanov, P.R. Munroe, FIB-induced damage in silicon, J. Microsc. 214 (3) (2004) 213–221. http://dx.doi.org/10.1111/j.0022-2720.2004.01327.x.
[16] J. Hütsch, E.T. Lilleodden, The influence of focused-ion beam preparation technique on microcompression investigations: lathe vs. annular milling, Scr. Mater. 77 (2014) 49–51. http://dx.doi.org/10.1016/j.scriptamat.2014.01.016.
[17] S. Wurster, M. Jenko, C. Motz, R. Pippan, Micrometer-sized specimen preparation based on ion slicing technique, Adv. Eng. Mater. 12 (1) (2010) 61–64. http://dx.doi.org/10.1002/adem.200900263.
[18] N.S. Smith, W.P. Skoczylas, S.M. Kellogg, D.E. Kinion, P.P. Tesch, O. Sutherland, A. Aanesland, R.W. Boswell, High brightness inductively coupled plasma source for high current focused ion beam applications, J. Vac. Sci. Technol. B 24 (6) (2006) 2902–2906. http://dx.doi.org/10.1116/1.2366617.
[19] L. Kwakman, G. Franz, M. Taklo, A. Klumpp, P. Ramm, Characterization and Failure Analysis of 3D Integrated Systems using a Novel Plasma-FIB System, Frontiers of Characterization and Metrology for Nanoelectronics: 2011, Vol. 1395, 2011, pp. 269–273. http://dx.doi.org/10.1063/1.3657902.
[20] L. Kwakman, M. Straw, G. Coustillier, M. Sentis, J. Beyersdorfer, J. Schischka, F. Naumann, F. Altmann, Sample Preparation Strategies for Fast and Effective Failure Analysis of 3D Devices, ISTFA 2013: Proceedings from the 39th International Symposium for Testing and Failure Analysis, ASM International. 2013, pp. 17–26.
[21] Y. Xiao, J. Wehrs, H. Ma, T. Al-Samman, S. Korte-Kerzel, M. Gken, J. Michler, R. Spolenak, J.M. Wheeler, Investigation of the deformation behavior of aluminum micropillars produced by focused ion beam machining using Ga and Xe ions, ResearchGate (2016) http://dx.doi.org/10.1016/j.scriptamat.2016.08.028.
[22] T. Kawakami, M. Kunieda, Study on factors determining limits of minimum machinable size in micro EDM, CIRP Ann. Manuf. Technol. 54 (1) (2005) 167–170. http://dx.doi.org/10.1016/S0007-8506(07)60075-4.
[23] N. Schmitt, C. Bohnert, C. Eberl, R. Schwaiger, S. Weygand, O. Kraft, Investigation of the fracture behavior of tungsten at the micro scale, ICF Proceedings 13th International Conf. on Fracture, Beijing. 2013, 3342–3349.
[24] M.D. Uchic, D.M. Dimiduk, A methodology to investigate size scale effects in crystalline plasticity using uniaxial compression testing, Mater. Sci. Eng. A 400401 (2005) 268–278. http://dx.doi.org/10.1016/j.msea.2005.03.082.
[25] N. Mohd Abbas, D.G. Solomon, M. Fuad Bahari, A review on current research trends in electrical discharge machining (EDM), Int. J. Mach. Tools Manuf. 47 (78) (2007) 1214–1228. http://dx.doi.org/10.1016/j.ijmachtools.2006.08.026.
[26] M.G. Cohen, R.A. Kaplan, E.G. Arthurs, Micro-materials processing, Proc. IEEE 70 (6) (1982) 545–555. http://dx.doi.org/10.1109/PROC.1982.12353.
[27] M.P. Echlin, M. Straw, S. Randolph, J. Filevich, T.M. Pollock, The TriBeam system: femtosecond laser ablation in situ SEM, Mater. Charact. 100 (2015) 1–12. http://dx.doi.org/10.1016/j.matchar.2014.10.023.
[28] B.N. Chichkov, C. Momma, S. Nolte, F. v. Alvensleben, A. Tünnermann, Femtosecond, picosecond and nanosecond laser ablation of solids, Appl. Phys. A 63 (2) (1996) 109–115. http://dx.doi.org/10.1007/BF01567637.
[29] X. Liu, D. Du, G. Mourou, Laser ablation and micromachining with ultrashort laser pulses, IEEE J. Quantum Electron. 33 (10) (1997) 1706–1716. http://dx.doi.org/10.1109/3.631270.

[30] K. Sugioka, Progress in ultrafast laser processing and future prospects, Nanophotonics 5 (2016) 17–37. http://dx.doi.org/10.1515/nanoph-2016-0004.
[31] E. Mottay, X. Liu, H. Zhang, E. Mazur, R. Sanatinia, W. Pfleging, Industrial applications of ultrafast laser processing, MRS Bull. 41 (12) (2016) 984–992.
[32] P. Lu, R.J.K. Wood, M.G. Gee, L. Wang, W. Pfleging, The friction reducing effect of square-shaped surface textures under lubricated line-contacts - an experimental study, Lubricants 4 (3) (2016) 26. http://dx.doi.org/10.3390/lubricants4030026.
[33] M.P. Echlin, M.S. Titus, M. Straw, P. Gumbsch, T.M. Pollock, Materials response to glancing incidence femtosecond laser ablation, Acta Mater. 124 (2017) 37–46. http://dx.doi.org/10.1016/j.actamat.2016.10.055.
[34] K.M.T. Ahmmed, C. Grambow, A.-M. Kietzig, Fabrication of micro/nano structures on metals by femtosecond laser micromachining, Micromachines 5 (4) (2014) 1219–1253. http://dx.doi.org/10.3390/mi5041219.
[35] A.Y. Vorobyev, C. Guo, Colorizing metals with femtosecond laser pulses, Appl. Phys. Lett. 92 (4) (2008) 041914. http://dx.doi.org/10.1063/1.2834902.
[36] M. Halbwax, T. Sarnet, P. Delaporte, M. Sentis, H. Etienne, F. Torregrosa, V. Vervisch, I. Perichaud, S. Martinuzzi, Micro and nano-structuration of silicon by femtosecond laser: application to silicon photovoltaic cells fabrication, Thin Solid Films 516 (20) (2008) 6791–6795. http://dx.doi.org/10.1016/j.tsf.2007.12.117.
[37] G. Kamlage, T. Bauer, A. Ostendorf, B.N. Chichkov, Deep drilling of metals by femtosecond laser pulses, Appl Phys A 77 (2) (2003) 307–310. http://dx.doi.org/10.1007/s00339-003-2120-x.
[38] K. Furusawa, K. Takahashi, H. Kumagai, K. Midorikawa, M. Obara, Ablation characteristics of Au, Ag, and Cu metals using a femtosecond Ti:sapphire laser, Appl Phys A 69 (1) (1999) S359–S366. http://dx.doi.org/10.1007/s003390051417.
[39] S. Ma, J.P. McDonald, B. Tryon, S.M. Yalisove, T.M. Pollock, Femtosecond laser ablation regimes in a single-crystal superalloy, Metall and Mat Trans A 38 (13) (2007) 2349–2357. http://dx.doi.org/10.1007/s11661-007-9260-0.
[40] N. Naderi, S. Legacey, S.L. Chin, Preliminary investigations of ultrafast intense laser wood processing, For. Prod. J. 49 (1999) 72–76.
[41] Y.C. Lim, K.J. Altman, D.F. Farson, K.M. Flores, Micropillar fabrication on bovine cortical bone by direct-write femtosecond laser ablation, J. Biomed Opt 14 (6) (2009) 064021. http://dx.doi.org/10.1117/1.3268444.
[42] M.D. Perry, B.C. Stuart, P.S. Banks, M.D. Feit, V. Yanovsky, A.M. Rubenchik, Ultrashort-pulse laser machining of dielectric materials, J. Appl. Phys. 85 (9) (1999) 6803–6810. http://dx.doi.org/10.1063/1.370197.
[43] N. Bärsch, K. Körber, A. Ostendorf, K.H. Tönshoff, Ablation and cutting of planar silicon devices using femtosecond laser pulses, Appl. Phys A 77 (2) (2003) 237–242. http://dx.doi.org/10.1007/s00339-003-2118-4.
[44] T. Kim, H.S. Kim, M. Hetterich, D. Jones, J.M. Girkin, E. Bente, M.D. Dawson, Femtosecond laser machining of gallium nitride, Mater. Sci. Eng. B 82 (13) (2001) 262–264. http://dx.doi.org/10.1016/S0921-5107(00)00790-X.
[45] Z.B. Wang, M.H. Hong, Y.F. Lu, D.J. Wu, B. Lan, T.C. Chong, Femtosecond laser ablation of polytetrafluoroethylene (Teflon) in ambient air, J. Appl. Phys. 93 (10) (2003) 6375–6380. http://dx.doi.org/10.1063/1.1568154.
[46] J. Bonse, J. Krüger, S. Höhm, A. Rosenfeld, Femtosecond laser-induced periodic surface structures, J. Laser Appl. 24 (4) (2012) 042006. http://dx.doi.org/10.2351/1.4712658.
[47] O. Varlamova, F. Costache, M. Ratzke, J. Reif, Control parameters in pattern formation upon femtosecond laser ablation, Appl. Surf. Sci. 253 (19) (2007) 7932–7936. http://dx.doi.org/10.1016/j.apsusc.2007.02.067.
[48] M.P. Echlin, A. Mottura, C.J. Torbet, T.M. Pollock, A new TriBeam system for three-dimensional multimodal materials analysis, Rev. Sci. Instrum. 83 (2) (2012) 023701. http://dx.doi.org/10.1063/1.3680111.
[49] W. Zhao, P. Rao, Z. Ling, A new method for the preparation of ultra-sharp V-notches to measure fracture toughness in ceramics, J. Eur. Ceram. Soc. 34 (15) (2014) 4059–4062. http://dx.doi.org/10.1016/j.jeurceramsoc.2014.05.021.
[50] T. Palacios, J.Y. Pastor, Influence of the notch root radius on the fracture toughness of brittle metals: nanostructure tungsten alloy, a case study, Int. J. Refract. Met. Hard Mater. 52 (2015) 44–49. http://dx.doi.org/10.1016/j.ijrmhm.2015.05.012.
[51] R. Salzer, H. Stegmann, Efficient and precise sample preparation by combination of pulsed laser ablation and FIB milling, Microsc. Microanal. 18 (S2) (2012) 636–637. http://dx.doi.org/10.1017/S143192761200503X.
[52] J.M. Liu, Simple technique for measurements of pulsed Gaussian-beam spot sizes, Opt. Lett., OL 7 (5) (1982) 196–198. http://dx.doi.org/10.1364/OL.7.000196.
[53] J. Byskov-Nielsen, J.-M. Savolainen, M.S. Christensen, P. Balling, Ultra-short pulse laser ablation of metals: threshold fluence, incubation coefficient and ablation rates, Appl. Phys. A 101 (1) (2010) 97–101. http://dx.doi.org/10.1007/s00339-010-5766-1.
[54] E.G. Gamaly, A.V. Rode, B. Luther-Davies, V.T. Tikhonchuk, Ablation of solids by femtosecond lasers: ablation mechanism and ablation thresholds for metals and dielectrics, Phys. Plasmas 9 (3) (2002) 949–957. http://dx.doi.org/10.1063/1.1447555.
[55] L.M. Cabalín, J.J. Laserna, Experimental determination of laser induced breakdown thresholds of metals under nanosecond Q-switched laser operation, Spectrochim. Acta 53 (1998) 723–730. http://dx.doi.org/10.1016/S0584-8547(98)00107-4.
[56] J. Reiser, M. Rieth, A. Möslang, B. Dafferner, A. Hoffmann, X. Yi, D.E.J. Armstrong, Tungsten foil laminate for structural divertor applications tensile test properties of tungsten foil, J. Nucl. Mater. 434 (13) (2013) 357–366. http://dx.doi.org/10.1016/j.jnucmat.2012.12.003.
[57] I. Utke, S. Moshkalev, P. Russell, Nanofabrication Using Focused Ion and Electron Beams: Principles and Applications, Oxford University Press, USA, 2012.
[58] M.E. Shaheen, J.E. Gagnon, B.J. Fryer, Laser ablation of iron: a comparison between femtosecond and picosecond laser pulses, J. Appl. Phys. 114 (8) (2013) 083110. http://dx.doi.org/10.1063/1.4819804.